ADVANCED ENERGY MATERIALS
www.advenergymat.de

Graphene/*h*-BN Heterostructures: Recent Advances in Controllable Preparation and Functional Applications

Xiuju Song, Jingyu Sun, Yue Qi, Teng Gao, Yanfeng Zhang, and Zhongfan Liu**

Vertical heterostructures based on two-dimensional (2D) layered materials such as graphene and hexagonal boron nitride have emerged as a new paradigm of functional materials. Representing the thinnest and most commonplace 2D heterostructures, graphene/*h*-BN, have recently attracted considerable attentions due to their remarkable morphological, electrical, and thermal properties. Herein, this research news highlights recent advances in the preparation of graphene/*h*-BN heterostructures, especially via two representative routes involving the one-batch chemical vapor deposition and co-segregation growth methods. Furthermore, several promising applications of such heterostructures in energy-efficient nanoelectronics, energy conversion as well as energy harvesting are also introduced. The existing challenges and future directions with respect to the controllable preparation and the related applications of such graphene/*h*-BN heterostructures are finally proposed.

1. Introduction

Two-dimensional (2D) materials, such as graphene, hexagonal boron nitride (*h*-BN), and transition metal dichalcogenides (TMDCs, MX_2, X = W, Mo, X = Se, S) have received great attention lately since they have exhibited novel properties different from their corresponding bulk counterparts, such as quantum hall effect, superconductivity, charge density wave, and Shubnikov-de Haas oscillation, etc.[1–5] Progressively, developing van der Waals (vdW) heterostructures by vertically stacking such 2D layers, provides quite new properties and versatile applications beyond their single component.[6–10] As the most commonplace 2D vertical heterostructures, graphene/hexagonal boron nitride (denoted as G/*h*-BN), have stimulated extensive interest since its construction by Dean et al. in 2010 by a layer-by-layer transfer method.[11] Subsequently, they have acted as prototype systems for exploring some novel physics issues, such as commensurate-incommensurate transitions and Hofstadter's butterfly effect.[12–16] More significantly, such heterostructures have also dramatically stimulated the applications of graphene in nanoelectronics, photo-detection, and energy harvesting/conversion.[11,17–23] As an example, G/*h*-BN heterostructures have yielded so far the carrier mobilities as high as 350 000 $cm^2 V^{-1} s^{-1}$, owing to the atomically flat and dangling-bond-free feature of *h*-BN that greatly avoids the interface charge transfer.[11,17,18]

Securing reliable and robust methods for fabricating large area, high quality, stacking geometry controllable heterostructures becomes the most significant step for related fields. To date, three typical strategies have been developed to produce G/*h*-BN heterostructures, including layer-by-layer transfer of separately exfoliated 2D layers,[11,17,24–26] chemical vapor deposition (CVD) via an epitaxial mechanism,[27–32] and co-segregation from solid C and BN precursors.[33] Of particular note, the latter two methods have just been established in the last two years. Obviously, the layer-by-layer stacking of exfoliated materials can afford high-quality samples suitable for proof-of-concept device fabrications, whilst CVD and co-segregation routes are promising for the large-scale, thickness uniform, interface-clean, stacking geometry controllable synthesis of G/*h*-BN, mainly mediated by a vdW epitaxy mechanism.

In this research news, we highlight the recent development towards the fabrication, characterization, as well as versatile applications in energy-efficient nanoelectronics and energy conversion/harvesting of the G/*h*-BN heterostructures. We aim to provide a broad, but not exhaustive summary of the latest advances in this exciting field. We conclude with the main challenges and possible opportunities that researchers in this field are facing.

2. Overview of Controllable Preparation of G/*h*-BN Heterostructures

Preparing G/*h*-BN heterostructures is at current a hot issue with growing interests. Several reliable methods have been

Dr. X. Song, Dr. Y. Qi, Prof. Y. Zhang, Prof. Z. Liu
Center for Nanochemistry (CNC)
Beijing National Laboratory for Molecular Sciences
College of Chemistry and Molecular Engineering
Academy for Advanced Interdisciplinary Studies
Peking University
Beijing 100871, P. R. China
E-mail: yanfengzhang@pku.edu.cn; zfliu@pku.edu.cn
Prof. Y. Zhang
Department of Materials Science and Engineering
College of Engineering
Peking University
Beijing 100871, P. R. China
Dr. J. Sun
Cambridge Graphene Centre
Department of Engineering
University of Cambridge
9 JJ Thomson Avenue, Cambridge CB3 0FA, UK
Dr. T. Gao
Department of Chemistry and Chemical Biology
Harvard University
Cambridge, MA 02138, USA

DOI: 10.1002/aenm.201600541

 © 2016 WILEY-VCH Verlag GmbH & Co. KGaA, Weinheim

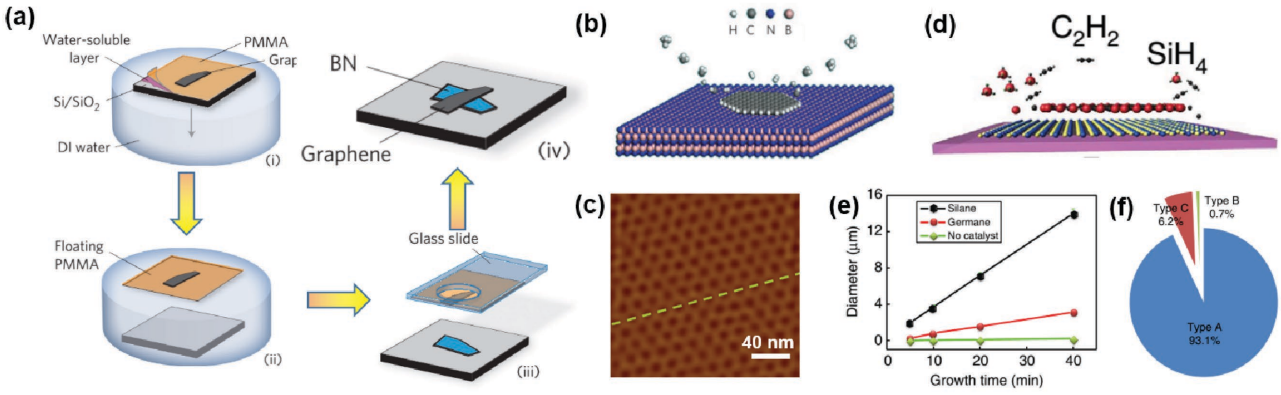

Figure 1. G/*h*-BN preparation: layer-by-layer transfer method and typical CVD route regarding direct synthesis of graphene on exfoliated *h*-BN. (a) Schematic illustration of layer-by-layer transfer of separate *h*-BN and graphene flakes. Reproduced with permission.[11] Copyright 2010, Nature Publishing Group. (b,c) Schematic illustration of the epitaxial growth of graphene on exfoliated *h*-BN by a remote plasma-enhanced CVD route, with the AFM image of the as-grown sample showing a periodic moiré pattern of ≈14 nm. Reproduced with permission.[28] Copyright 2013, Nature Publishing Group. (d) Schematic illustration of the gaseous catalyst-assisted CVD process. Reproduced with permission.[29] Copyright 2015, Nature Publishing Group. (e) Growth duration dependence of the domain sizes for single-crystalline graphene using silane (black) or germane (red) gaseous catalysts and without catalyst (green), respectively. Reproduced with permission.[29] Copyright 2015, Nature Publishing Group. (f) Distribution of the type of graphene domains obtained with the presence of silane. Type A, B, and C indicates G/*h*-BN with precise alignment, 30° rotation and polycrystalline structure, respectively. Reproduced with permission.[29] Copyright 2015, Nature Publishing Group.

developed in the past few years, including the layer-by-layer transfer, the direct CVD synthesis method, as well as the co-segregation of graphene and *h*-BN layers. This section mainly highlights the recent advances in the fabrication of G/*h*-BN heterostructures, particularly focusing on the CVD-related synthesis routes.

2.1. Layer-by-Layer Transfer of Graphene and *h*-BN Flakes

The pioneering work in the preparation of G/*h*-BN heterostructures (as illustrated in **Figure 1**a) was reported by Dean et al. via a layer-by-layer transfer method.[11] In this method, mechanically cleaved *h*-BN flake was deposited on SiO_2/Si, whilst cleaved graphene flake was firstly deposited on a polymer stack (coating on SiO_2/Si) consisting of a poly(methyl methacrylate) (PMMA) and a water-soluble layer. After detaching from the Si substrate, a glass slide was used to adhere and support the graphene/PMMA and subsequently transfer it on top of a targeted *h*-BN flake. The control of graphene locations can be realized with the aid of an optical microscope. Based on this work, several routes have been developed by modifying the different procedures, such as with the aid of an optical mask[25] or via a dry transfer technique,[34] respectively. By using the layer-by-layer transfer method, CVD-grown 2D films were also utilized to construct G/*h*-BN, i.e., by transferring CVD-grown graphene on exfoliated *h*-BN[24] or stacking CVD-grown graphene onto CVD-grown *h*-BN films,[35] respectively. Notably, such layer-by-layer transfer method is featured by its ease-of-operation and relatively high sample quality, making it an ideal route for fundamental studies. However, its lack of sophisticated control over the domain size, shape and orientation, as well as the unavoidable adsorbates at interfaces usually deteriorates the intrinsic properties of heterostructures.[7,36]

2.2. Direct Chemical Vapor Deposition Growth of Graphene on Exfoliated *h*-BN

The CVD technique has become the most prevailing route for synthesizing 2D materials, because it has the potential to produce large scale, high purity, large domain, and thickness uniform 2D layers. Earlier attempts were mainly concerned with using exfoliated *h*-BN as a substrate for graphene CVD growth, since the exfoliated few layer *h*-BN was readily available by the exfoliation method, and they could serve as good dielectric layers in related devices. However, exfoliated *h*-BN (normally placed on SiO_2) appears to have insufficient catalytic capabilities for the subsequent graphene growth.[37–39] Very recently, special attentions have been paid to exploring the detailed CVD processes, and several intriguing results have been presented.

Zhang et al. selected energetic plasma to aid the dissociation of the carbon feedstock and realized the vdW epitaxial growth of single-crystalline graphene flakes on exfoliated *h*-BN (Figure 1b).[28] Raman spectra confirmed the stacking sequence of graphene on *h*-BN, as well as the relatively high crystal quality and thickness uniformity of graphene. The long-period moiré pattern (≈14 nm) shown in the high-resolution atomic force microscopy (AFM) image suggested the nearly identical orientation of graphene and *h*-BN lattice (Figure 1c). Corresponding electronic device measurements showed a relatively high mobility of ≈5000 $cm^2\ V^{-1}\ s^{-1}$ at 1.5 K and the half-integer quantum Hall effect. All these data verified the reliability of the plasma-enhanced CVD route for G/*h*-BN synthesis.

Later on, Xie et al. found that gaseous catalysts such as silane and germane can surprisingly boost the growth rate of graphene on pre-deposited, mechanically exfoliated *h*-BN, leading to the growth of single crystal graphene domains of ≈20 μm (in edge length) within only 20 min growth time (Figure 1d and e).[29] Indeed, the graphene growth rate on *h*-BN using silane as a catalyst increased by two orders of magnitude as compared to

© 2016 WILEY-VCH Verlag GmbH & Co. KGaA, Weinheim

the scenario with no catalyst. In addition, the presence of gaseous catalyst enhanced the alignment of graphene with *h*-BN compared to that lacking of catalysts (Figure 1f). The carrier mobility of the related devices reached as high as 20 000 cm^2 V^{-1} s^{-1} at room temperature. Furthermore, theoretical calculations revealed that the introduction of Si atoms to the growth front of graphene can effectively reduce the threshold barrier for the incorporation of carbon species onto a graphene edge to form a new hexagon nucleus, and result in the dramatic increase of the growth rate.

2.3. One-Batch Chemical Vapor Deposition Growth of G/*h*-BN Heterostructures

As compared to aforementioned methods involving CVD growth of graphene on transferred *h*-BN substrates, one-batch, all-CVD route is advantageous for avoiding any transfer-induced contaminants and defects, as well as bypassing the size limitation of the exfoliated *h*-BN substrates. Lee et al. managed to directly grow graphene on few-layer, CVD-grown *h*-BN throughout an all-CVD route (**Figure 2**a),[30] as confirmed by Raman spectra showing the monolayer nature of the overlying graphene layer. More importantly, further comparisons of the electrical properties between the all-CVD derived and the transferred G/*h*-BN indicated that the direct CVD sample possessed a rather clean interface. Followed-up work by the same group was concerned with the CVD growth of graphene on *h*-BN with different thickness on Cu foils, where the *h*-BN was obtained by CVD and stacked on Cu by transfer. It was intriguing to find that a relatively thin *h*-BN/Cu was more catalytically transparent on the graphene growth, as compared to that of thick *h*-BN layers (Figure 2b).[31]

During the sequential growth of *h*-BN and graphene, the pre-deposited *h*-BN layer is possibly etched by the H- and/or O-containing gaseous species in the second growth of graphene.[40] To overcome or even take advantage of this phenomenon, Liu et al. maneuvered the feedstock chemistry and achieved the selective

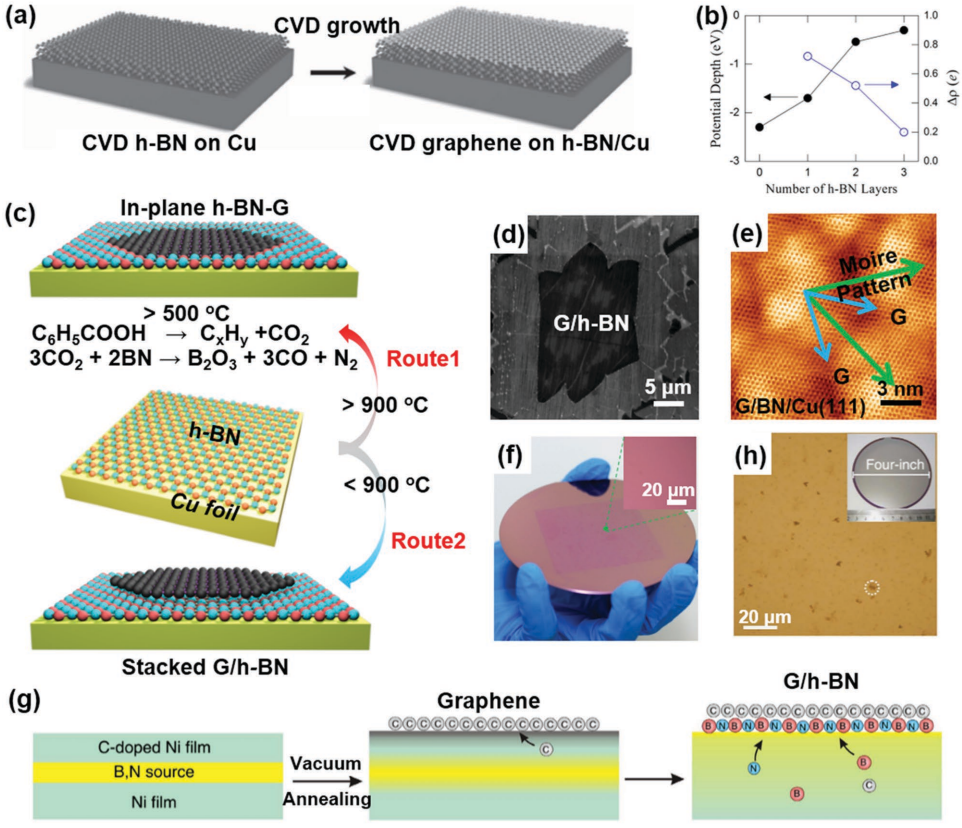

Figure 2. G/*h*-BN preparation: one-batch CVD and co-segregation routes. (a) Schematic diagram of graphene growth on multilayer *h*-BN/Cu at 1000 °C with CH_4 as carbon source. Reproduced with permission.[30] Copyright 2013, Wiley. (b) Potential depth (solid circles) and charge profile (open circles) of CH_3 on *h*-BN/Cu(111) versus the number of *h*-BN atomic layers. Reproduced with permission.[31] Copyright 2014, American Chemical Society. (c) Schematic illustration of the temperature-triggered switching growth between in-plane *h*-BN-G and stacked G/*h*-BN heterostructures by using benzoic acid as carbon source, defined as Route 1 (900 °C) and Route 2 (850 °C), respectively. Reproduced with permission.[27] Copyright 2015, Nature Publishing Group. (d) SEM image of graphene domain up to ≈20 μm on *h*-BN/Cu. Reproduced with permission.[27] Copyright 2015, Nature Publishing Group. (e) High-resolution STM image (V_b = –0.002 V, I_t = 10.785 nA) showing a ≈7.8 nm period of moiré pattern, indicating the precisely alignment. Reproduced with permission.[27] Copyright 2015, Nature Publishing Group. (f) Photograph of large-scale G/*h*-BN film transferred onto the 4-inch SiO_2/Si wafer with an optical microscopy image as the inset. Reproduced with permission.[27] Copyright 2015, Nature Publishing Group. (g) Schematic illustration of the co-segregation growth process of G/*h*-BN heterostructures. Reproduced with permission.[33] Copyright 2015, Nature Publishing Group. (h) Optical image of the as-grown sample after annealing at 950 °C for 10 min with the inset displaying a four-inch wafer sample. Reproduced with permission.[33] Copyright 2015, Nature Publishing Group.

© 2016 WILEY-VCH Verlag GmbH & Co. KGaA, Weinheim

synthesis of vertically stacked or in-plane heterostructures by a temperature-triggered one-batch CVD method with benzoic acid carbon precursors.[27] The entire process began with the growth of monolayer *h*-BN film on Cu foils by using ammonia borane as BN precursors. For the subsequent graphene growth, the reaction temperature was found to be a key parameter for tuning the growth trend, since benzoic acid can decompose into CO_2, which would etch away *h*-BN above 900 °C leading to the exposure of bare Cu, due to the chemical reaction between CO_2 and *h*-BN. Consequently, the graphene growth above or below 900 °C gave rise to the target synthesis of in-plane *h*-BN-G or vertically stacked G/*h*-BN heterostructures (Route 1 or 2, Figure 2c), respectively.

Furthermore, this all-CVD route enabled the effective control over the single crystal size (as large as ≈20 μm) and the coverage of graphene on *h*-BN (from sub-monolayer to complete monolayer, Figure 2d,f). In-depth characterizations by scanning tunneling microscopy (STM) (Figure 2e) revealed good alignment of graphene with *h*-BN, as evidenced by a uniform moiré period of 7.45 nm. Additionally, the batch production of G/*h*-BN was also available with the current all-CVD method (Figure 2f), which should greatly advance its applications in various aspects.

2.4. Co-Segregation Growth of G/*h*-BN with the Utilization of C and BN Precursors

Inspired by their previous work regarding the segregation growth of graphene,[41] Liu et al. devised a co-segregation route to directly fabricate G/*h*-BN heterostructures on Ni films.[33] This synthesis route was based on a sandwiched substrate of Ni(C)/(B, N)/Ni constructed by sequentially e-beam evaporating Ni, BN and C-doped Ni films (Figure 2g). High-temperature annealing process was then applied to the sandwich under high vacuum conditions. Dissolved C firstly segregated on the top of the C-doped Ni films with the formation of graphene. The trapped B and N sources were concurrently diffused into the interface of graphene and Ni films to form *h*-BN layers (Figure 2g). Detailed characterizations with optical microscopy, Raman spectroscopy, and high-resolution transmission electron microscopy confirmed that as-grown graphene possessed tunable thicknesses ranging from monolayer to few-layer. Amazingly, this unique segregation approach enabled the large-scale synthesis of G/*h*-BN heterostructures (4-inch wafer sample, Figure 2h).

Table 1 summarizes the preparation methodology of G/*h*-BN heterostructures. In essence, mechanical transfer technique is ideal for fundamental studies, however, several issues such as limited sample sizes, surface/interface contaminants, sophisticated handling, and poor alignment controllability strongly hinder its practical applications. The CVD method is suitable for the large-scale production of G/*h*-BN heterostructures, although further increasing the graphene domain size, the thickness uniformity, as well as the stacking registry remain to be tackled. Co-segregation approach paves another scalable route towards the batch production of G/*h*-BN heterostructures, although process optimization is required to avoid the doping of graphene by B and N atoms. As such, significant synthetic efforts should be undertaken to ultimately realize the combination of production quality control with wafer-level scalability. Furthermore, it is worth-mentioning that these techniques, in particular CVD routes, have been widely utilized for realizing tailored preparation of other types of 2D heterostructures, such as MoS_2/graphene,[42] MoS_2/*h*-BN,[43] MoS_2/WS_2,[44] etc.

3. Promising Applications Based on G/*h*-BN Heterostructures

The realization of controllable fabrication of G/*h*-BN heterostructures is of paramount importance to the rational exploration of unique properties and potential applications of such specific hybrids. In this section, several functional applications of G/*h*-BN are highlighted.

It is well known that the performances of graphene based nanoelectronic devices can be greatly degraded by carrier scattering, originating from large surface roughnesses, charge traps, and foreign contaminants on conventional substrates (such as SiO_2). In this regard, *h*-BN was proved to be perfect substrate/gate insulator materials for improving the transport properties of graphene because of its dangling-bond-free, ultra-flat surface, as well as dielectric nature. Crommie et al. presented rather uniform charge density for G/*h*-BN/SiO_2 with regard to that of G/SiO_2 by using STM (**Figure 3**a), thus providing direct evidence that *h*-BN was a perfect substrate for graphene electronics as compared to that of SiO_2.[17] Dean and colleagues fabricated devices using mechanically transferred G/*h*-BN heterostructures on SiO_2 and found that graphene on *h*-BN showed a three-fold increase in carrier mobility (60 000 $cm^2 V^{-1} s^{-1}$) as compared to that on SiO_2 (Figure 3b).[11] Notably, rather than a broad resistivity peak and heavy doping of graphene on SiO_2 (Figure 3c), graphene on *h*-BN exhibited an extremely narrow resistivity peak and nearly no doping

Table 1. Summary of the preparation methodology for G/*h*-BN heterostructures.

Methods	Substrate	Scale	Quality	Thickness	Interface contamination	Relative orientation	Carrier mobility ($cm^2 V^{-1} s^{-1}$)
Layer-by-Layer transfer	Exfoliated *h*-BN	Limited by *h*-BN	High	1L, 2L, multilayer	Residue or water	Multiple (needs skilled operation)	350 000[18]
CVD Growth	Exfoliated *h*-BN	Limited by *h*-BN	Fair	1L, 2L, multilayer	Clean	Predominantly aligned	20 000[29]
	CVD-grown *h*-BN	Wafer-scale	Fair	1L	Clean	Predominantly aligned	15 000[27]
Co-segregation	Ni film	Wafer-scale	Heavy doping	1L, 2L, multilayer	Clean	Multiple (0°, 11°, etc.)	1.5[33]

© 2016 WILEY-VCH Verlag GmbH & Co. KGaA, Weinheim

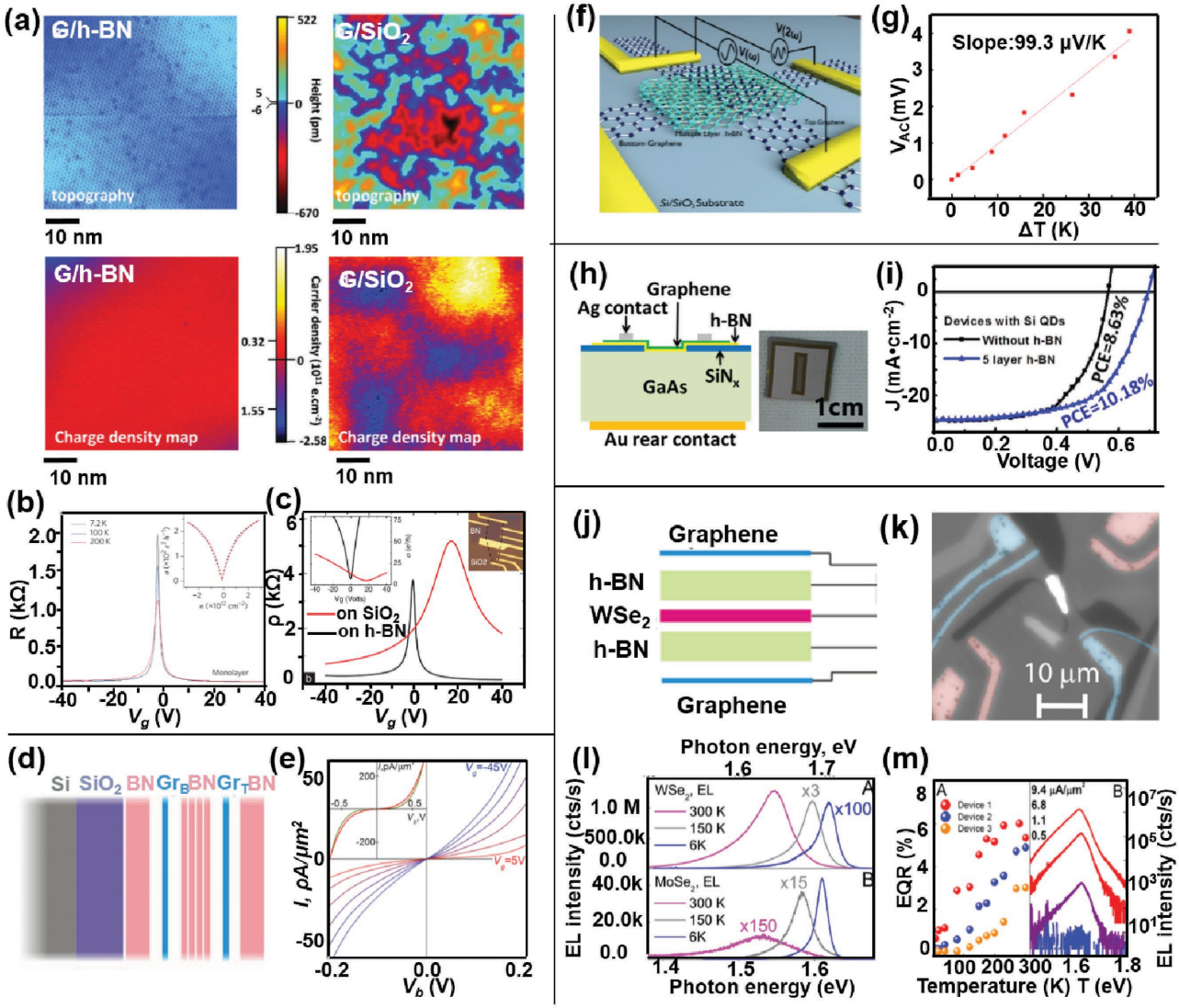

Figure 3. Functional applications based on G/*h*-BN heterostructures. (a) STM topography of G/*h*-BN (upper left, $I_t = 0.2$ nA, $V_b = 0.25$ V, $V_G = 6$ V) and G/SiO_2 (upper right, $I_t = 0.02$ nA, $V_b = 0.225$ V, $V_G = 15$ V) with their corresponding charge density maps of G/*h*-BN (bottom left) and G/SiO_2 (bottom right), respectively. Reproduced with permission.[17] Copyright 2011, American Chemical Society. (b) Resistance versus applied gate voltage for monolayer graphene, with the inset showing the corresponding conductivity. Reproduced with permission.[11] Copyright 2010, Nature Publishing Group. (c) Resistivity measured on a single flake spanning both BN and SiO_2 substrate regions. The inset shows corresponding conductivity (left) and optical image of the sample (right). Reproduced with permission.[11] Copyright 2010, Nature Publishing Group. (d) Schematic illustrations of graphene quantum tunneling transistors. Reproduced with permission.[19] Copyright 2012, American Association for the Advancement of Science. (e) I-V_sV_s curve for different V_g (in 10 V steps). Reproduced with permission.[19] Copyright 2012, American Association for the Advancement of Science. (f) Schematic diagram of the graphene/*h*-BN/graphene/Al_2O_3 heterostructure device and measurement setup. Reproduced with permission.[21] Copyright 2015, Springer. (g) 400 Hz thermoelectric voltage as a function of the maximum possible temperature drop (ΔT) across the heterostructure. Reproduced with permission.[21] Copyright 2015, Springer. (h) Left: Schematic of the G/*h*-BN/GaAs sandwich device. Right: Digital photograph of one typical device. Reproduced with permission.[22] Copyright 2016, The Optical Society. (i) Typical dark current density-voltage (J–V) curves of solar cells based on G/GaAs and G/*h*-BN/GaAs heterostructures with Si-QDs-introduced photo-induced doping. Reproduced with permission.[22] Copyright 2016, The Optical Society. (j) Schematic of vdW LED. Reproduced with permission.[23] Copyright 2015, American Chemical Society. (k) Magnification (50×) monochrome image of a WSe_2 light-emitting quantum well device with an applied bias of $V_b = 2$ V and current of 2 μA taken in ambient conditions with weak backlight illuminations (central white area corresponds to strong electroluminescence). Reproduced with permission.[23] Copyright 2015, American Chemical Society. (l) Electroluminescence spectra taken at different temperatures for a WSe_2 (up) and $MoSe_2$ (down) quantum well. Reproduced with permission.[23] Copyright 2015, American Chemical Society. (m) Temperature-dependence of the quantum efficiency for three typical WSe_2 LED devices (left); individual electroluminescence spectra plotted for four different injection current densities (right). Reproduced with permission.[23] Copyright 2015, American Chemical Society.

effect. All these indicated that the G/*h*-BN heterostructures were promising for energy-efficient, low-voltage electronic applications.[17,24,25]

Recent years have indeed witnessed ever-growing research efforts on the development of electronic devices such as field-effect transistors and flexible thin-film transistors based on

© 2016 WILEY-VCH Verlag GmbH & Co. KGaA, Weinheim

Table 2. Summary of the applications based on G/*h*-BN heterostructures.

Heterostructures	Fields	Application	Reference
G/*h*-BN	Nanoelectronics	Field-effect transistor	[11]
G/*h*-BN/G	Nanoelectronics	Quantum tunneling transistor	[19]
G/*h*-BN/G	Energy conversion	Thermoelectric device	[21]
G/*h*-BN/GaAs	Energy harvesting	Solar cell	[22]
G/*h*-BN/MX_2/*h*-BN/G	Optoelectronics	LED	[23]

graphene.[45] However, one of the bottlenecks that impedes the application of graphene as an alternative to silicon is the absence of band-gap for graphene. As such, the graphene electronic devices display a poor ON–OFF ratio. Britnell et al. reported a new type of quantum tunneling transistor based on the G/*h*-BN structure, i.e., a *h*-BN tunnel barrier was encapsulated by ultrathin graphene electrodes (Figure 3d).[19] In such unique tunneling transistors, a current flow passed through the *h*-BN barrier by quantum tunneling effect when applied a bias voltage, managing to demonstrate a ON–OFF ratio of ≈50 at room temperature (Figure 3e), which is ten times larger than that of traditional planar graphene transistor. This specific device may find potential use in high-speed logical circuits.

In addition to energy-efficient electronics, emerging fields with respect to applications of G/*h*-BN heterostructures in energy conversion and harvesting, albeit at a nascent stage, have stimulated wide interests. Cronin et al. carried out thermoelectric transport measurements across graphene/*h*-BN/graphene sandwiches (Figure 3f), aiming to study the heat dissipation behaviors.[21] Evidently, such heterostructures yielded a higher Seebeck coefficient of ≈99.3 μV K^{-1} (Figure 3g) than that of the in-plane monolayer graphene (≈50 μV K^{-1}). This work may afford new possibility in the field of thermoelectric energy conversion using vdW heterostructures. Very recently, Lin et al. designed a sandwiched diode consisting of G/*h*-BN/GaAs layers (Figure 3h) for solar cell applications.[22] A rather high power conversion efficiency (≈10.18%) compared to that of conventional ones (≈8.63%) (Figure 3i) was achieved, possibly owing to the suppression of statistic charge transfer, as well as the increase of the barrier height with the presence of five layer *h*-BN. Moreover, with the combination of TMDC materials, Novoselov et al. developed a new type of light-emitting diode (LED) based on G/*h*-BN.[23,46] The LED encompassed an active TMDC semiconducting layer sandwiched into very thin insulating *h*-BN barriers, with graphene electrodes placing both on top and at bottom (Figure 3j,k). By investigating the performances using different TMDC materials such as MoS_2, $MoSe_2$, and WSe_2, it was concluded that the external light emission efficiency of WSe_2 devices reached 5% at room temperature (250-fold more than that of MoS_2 and $MoSe_2$), with the efficiency favorably comparable with that of the modern LEDs based on organic materials (Figure 3l,m). Such proof-of-concept LED devices could trigger the development of energy-saving wearable optoelectronics with the introduction of the novel G/*h*-BN heterostructures. **Table 2** summarizes the versatile applications of G/*h*-BN heterostructures in the fields of nanoelectronics, optoelectronics, as well as energy conversion and harvesting.

4. Conclusion and Outlook

In summary, the state-of-the-art research activities in the controlled preparation of G/*h*-BN heterostructures, including mechanical transfer technique, CVD synthetic route, and co-segregation method have been summarized. Particularly, the CVD route is found to be reliable for the batch production of high-quality G/*h*-BN heterostructures. Such heterostructures, once fabricated perfectly, can present great advantages in some promising application sectors, ranging from energy-efficient electronics, energy conversion and harvesting, as well as energy-saving optoelectronics.

Despite continuous advances made along this way during the past few years, the mass production of G/*h*-BN heterostructures with precise control over the quality and scalability remains at a nascent stage. Therefore, further research directions towards the scalable production of high quality G/*h*-BN are proposed. First of all, synthesizing high quality and thickness uniform *h*-BN layer is of fundamental importance in the all-CVD growth process, since the first 2D layer can dictate the perfection of the growth of a second layer.[7] In this regard, new fabricating technologies need to be developed for high-quality *h*-BN synthesis. Second, developing an epitaxial growth pathway is also essential for realizing the control over the orientation of graphene and *h*-BN lattices at a large scale, for the purpose of unraveling the unique electronic property and the new application potentials of G/*h*-BN. Thirdly, the co-segregation route indeed leads to facile and batch-scale synthesis of G/*h*-BN heterostructures, however, the current recipe usually gives rise to heavily doped graphene followed with rather low carrier mobility, and an optimized segregation pathway is highly desirable.

Acknowledgements

X.S., J.S., and Y.Q. contributed equally to this work. This work was financially supported by National Natural Science Foundation of China (Grants Nos. 51290272, 51472008, 51222201, 21201012, 51121091, 51072004, 51201069, 51520105003, and 51432002) and the Ministry of Science and Technology of China (Grants Nos. 2012CB921404, 2012CB933404, and 2013CB932603) and the Beijing Municipal Science and Technology Planning Project (No. Z151100003315013).

Received: March 11, 2016
Revised: March 26, 2016
Published online:

[1] K. S. Novoselov, A. K. Geim, S. V. Morozov, D. Jiang, Y. Zhang, S. V. Dubonos, I. V. Grigorieva, A. A. Firsov, *Science* **2004**, *306*, 666.
[2] Y. Zhang, Y. W. Tan, H. L. Stormer, P. Kim, *Nature* **2005**, *438*, 201.
[3] Y. M. Li, J. Li, L. K. Shi, D. Zhang, W. Yang, K. Chang, *Phys. Rev. Lett.* **2015**, *115*, 166804.
[4] B. Fallahazad, H. C. P. Movva, K. Kim, S. Larentis, T. Taniguchi, K. Watanabe, S. K. Banerjee, E. Tutuc, *Phys. Rev. Lett.* **2016**, *116*, 086601
[5] T. Ritschel, J. Trinckauf, K. Koepernik, B. Buchner, M. v. Zimmermann, H. Berger, Y. I. Joe, P. Abbamonte, J. Geck, *Nat. Phys.* **2015**, *11*, 328.

© 2016 WILEY-VCH Verlag GmbH & Co. KGaA, Weinheim

[6] A. K. Geim, I. V. Grigorieva, *Nature* **2013**, *499*, 419.
[7] J. A. Robinson, *ACS Nano* **2016**, *10*, 42.
[8] H. Wang, F. Liu, W. Fu, Z. Fang, W. Zhou, Z. Liu, *Nanoscale* **2014**, *6*, 12250.
[9] F. Withers, O. Del Pozo-Zamudio, A. Mishchenko, A. P. Rooney, A. Gholinia, K. Watanabe, T. Taniguchi, S. J. Haigh, A. K. Geim, A. I. Tartakovskii, K. S. Novoselov, *Nat. Mater.* **2015**, *14*, 301.
[10] X. Cui, G.-H. Lee, Y. D. Kim, G. Arefe, P. Y. Huang, C.-H. Lee, D. A. Chenet, X. Zhang, L. Wang, F. Ye, F. Pizzocchero, B. S. Jessen, K. Watanabe, T. Taniguchi, D. A. Muller, T. Low, P. Kim, J. Hone, *Nat. Nanotechnol.* **2015**, *10*, 534.
[11] C. R. Dean, A. F. Young, I. MericI, C. Lee, L. Wang, S. Sorgenfrei, K. WatanabeK, T. Taniguchi, P. Kim, K. L. Shepard, J. Hone, *Nat. Nanotechnol.* **2010**, *5*, 722.
[12] C. R. Dean, L. Wang, P. Maher, C. Forsythe, F. Ghahari, Y. Gao, J. Katoch, M. Ishigami, P. Moon, M. Koshino, T. Taniguchi, K. Watanabe, K. L. Shepard, J. Hone, P. Kim, *Nature* **2013**, *497*, 598.
[13] B. Hunt, J. D. Sanchez-Yamagishi, A. F. Young, M. Yankowitz, B. J. LeRoy, K. Watanabe, T. Taniguchi, P. Moon, M. Koshino, P. Jarillo-Herrero, R. C. Ashoori, *Science* **2013**, *340*, 1427.
[14] L. A. Ponomarenko, R. V. Gorbachev, G. L. Yu, D. C. Elias, R. Jalil, A. A. Patel, A. Mishchenko, A. S. Mayorov, C. R. Woods, J. R. Wallbank, M. Mucha-Kruczynski, B. A. Piot, M. Potemski, I. V. Grigorieva, K. S. Novoselov, F. Guinea, V. I. Fal'ko, A. K. Geim, *Nature* **2013**, *497*, 594.
[15] C. R. Woods, L. Britnell, A. Eckmann, R. S. Ma, J. C. Lu, H. M. Guo, X. Lin, G. L. Yu, Y. Cao, R. V. Gorbachev, A. V. Kretinin, J. Park, L. A. Ponomarenko, M. I. Katsnelson, Y. N. Gornostyrev, K. Watanabe, T. Taniguchi, C. Casiraghi, H. J. Gao, A. K. Geim, K. S. Novoselov, *Nat. Phys.* **2014**, *10*, 451.
[16] Z. G. Chen, Z. Shi, W. Yang, X. Lu, Y. Lai, H. Yan, F. Wang, G. Zhang, Z. Li, *Nat. Commun.* **2014**, *5*, 4461.
[17] R. Decker, Y. Wang, V. W. Brar, W. Regan, H. Z. Tsai, Q. Wu, W. Gannett, A. Zettl, M. F. Crommie, *Nano Lett.* **2011**, *11*, 2291.
[18] L. Banszerus, M. Schmitz, S. Engels, J. Dauber, M. Oellers, F. Haupt, K. Watanabe, T. Taniguchi, B. Beschoten, C. Stampfer, *Sci. Adv.* **2015**, *1*, e1500222.
[19] L. Britnell, R. V. Gorbachev, R. Jalil, B. D. Belle, F. Schedin, A. Mishchenko, T. Georgiou, M. I. Katsnelson, L. Eaves, S. V. Morozov, N. M. Peres, J. Leist, A. K. Geim, K. S. Novoselov, L. A. Ponomarenko, *Science* **2012**, *335*, 947.
[20] L. Britnell, R. V. Gorbachev, A. K. Geim, L. A. Ponomarenko, A. Mishchenko, M. T. Greenaway, T. M. Fromhold, K. S. Novoselov, L. Eaves, *Nat. Commun.* **2013**, *4*, 1794.
[21] C. C. Chen, Z. Li, L. Shi, S. B. Cronin, *Nano Res.* **2014**, *8*, 666.
[22] X. Li, S. Lin, X. Lin, Z. Xu, P. Wang, S. Zhang, H. Zhong, W. Xu, Z. Wu, W. Fang, *Opt. Express* **2016**, *24*, 134.
[23] F. Withers, O. Del Pozo Zamudio, S. Schwarz, S. Dufferwiel, P. M. Walker, T. Godde, A. P. Rooney, A. Gholinia, C. R. Woods, P. Blake, S. J. Haigh, K. Watanabe, T. Taniguchi, I. L. Aleiner, A. K. Geim, V. I. Fal'ko, A. I. Tartakovskii, K. S. Novoselov, *Nano Lett.* **2015**, *15*, 8223.
[24] W. Gannett, W. Regan, K. Watanabe, T. Taniguchi, M. F. Crommie, A. Zettl, *Appl. Phys. Lett.* **2011**, *98*, 242105.
[25] P. J. Zomer, S. P. Dash, N. Tombros, B. J. van Wees, *Appl. Phys. Lett.* **2011**, *99*, 232104.
[26] H. Xu, J. Wu, Y. Chen, H. Zhang, J. Zhang, *Chem. – Asian J.* **2013**, *8*, 2446.
[27] T. Gao, X. Song, H. Du, Y. Nie, Y. Chen, Q. Ji, J. Sun, Y. Yang, Y. Zhang, Z. Liu, *Nat. Commun.* **2015**, *6*, 6835.
[28] W. Yang, G. Chen, Z. Shi, C. C. Liu, L. Zhang, G. Xie, M. Cheng, D. Wang, R. Yang, D. Shi, K. Watanabe, T. Taniguchi, Y. Yao, Y. Zhang, G. Zhang, *Nat. Mater.* **2013**, *12*, 792.
[29] S. Tang, H. Wang, H. S. Wang, Q. Sun, X. Zhang, C. Cong, H. Xie, X. Liu, X. Zhou, F. Huang, X. Chen, T. Yu, F. Ding, X. Xie, M. Jiang, *Nat. Commun.* **2015**, *6*, 6499.
[30] M. Wang, S. K. Jang, W. J. Jang, M. Kim, S. Y. Park, S. W. Kim, S. J. Kahng, J. Y. Choi, R. S. Ruoff, Y. J. Song, S. Lee, *Adv. Mater.* **2013**, *25*, 2746.
[31] M. Wang, M. Kim, D. Odkhuu, N. Park, J. Lee, W. J. Jang, S. J. Kahng, R. S. Ruoff, Y. J. Song, S. Lee, *ACS Nano* **2014**, *8*, 5478.
[32] S. M. Kim, A. Hsu, P. T. Araujo, Y. H. Lee, T. Palacios, M. Dresselhaus, J. C. Idrobo, K. K. Kim, J. Kong, *Nano Lett.* **2013**, *13*, 933.
[33] C. Zhang, S. Zhao, C. Jin, A. L. Koh, Y. Zhou, W. Xu, Q. Li, Q. Xiong, H. Peng, Z. Liu, *Nat. Commun.* **2015**, *6*, 6519.
[34] J. A. Leon, N. C. Mamani, A. Rahim, L. E. Gomez, M. A. P. d. Silva, G. M. Gusev, *Graphene* **2014**, *3*, 25.
[35] L. Wang, B. Wu, J. Chen, H. Liu, P. Hu, Y. Liu, *Adv. Mater.* **2014**, *26*, 1559.
[36] H. Zhang, *ACS Nano* **2015**, *9*, 9451.
[37] X. Ding, G. Ding, X. Xie, F. Huang, M. Jiang, *Carbon* **2011**, *49*, 2522.
[38] M. Son, H. Lim, M. Hong, H. C. Choi, *Nanoscale* **2011**, *3*, 3089.
[39] S. Tang, G. Ding, X. Xie, J. Chen, C. Wang, X. Ding, F. Huang, W. Lu, M. Jiang, *Carbon* **2012**, *50*, 329.
[40] S. M. Kim, A. Hsu, P. T. Araujo, Y. H. Lee, T. Palacios, M. Dresselhaus, J. C. Idrobo, K. K. Kim, J. Kong, *Nano Lett.* **2013**, *13*, 933.
[41] N. Liu, L. Fu, B. Dai, K. Yan, X. Liu, R. Zhao, Y. Zhang, Z. Liu, *Nano Lett.* **2011**, *11*, 297.
[42] J. Shi, M. Liu, J. Wen, X. Ren, X. Zhou, Q. Ji, D. Ma, Y. Zhang, C. Jin, H. Chen, S. Deng, N. Xu, Z. Liu, Y. Zhang, *Adv. Mater.* **2015**, *27*, 7086.
[43] L. Fu, Y. Sun, N. Wu, R. G. Mendes, L. Chen, Z. Xu, T. Zhang, M. H. Rummeli, B. Rellinghaus, D. Pohl, L. Zhuang, L. Fu, *ACS Nano* **2016**, *10*, 2063.
[44] Y. Gong, J. Lin, X. Wang, G. Shi, S. Lei, Z. Lin, X. Zou, G. Ye, R. Vajtai, B. I. Yakobson, H. Terrones, M. Terrones, B. K. Tay, J. Lou, S. T. Pantelides, Z. Liu, W. Zhou, P. M. Ajayan, *Nat. Mater.* **2014**, *13*, 1135.
[45] D. Akinwande, N. Petrone, J. Hone, *Nat. Commun.* **2014**, *5*, 5678.
[46] X. Wang, F. Xia, *Nat. Mater.* **2015**, *14*, 264.

© 2016 WILEY-VCH Verlag GmbH & Co. KGaA, Weinheim